Similarity for High-Angle-of-Attack Subsonic/Transonic Slender-Body Aerodynamics

M. J. Hemsch*
PRC Aerospace Technologies Division, Hampton, Virginia

In a previous paper, it was shown that the similarity parameters deduced by Sychev for inviscid hypersonic flow over slender bodies could be used to accurately correlate the supersonic aerodynamic characteristics of thin slender wings and smooth slender bodies at low-to-high angles of attack. More importantly, the results showed that time-like behavior in the axial direction holds for arbitrary angles of attack provided the axial velocity component is supersonic and the flow features of interest are confined to a region near the body. In a recent note, Barnwell showed that Sychev's analysis could be applied to subsonic/transonic flows as well, provided that the outer-flow similarity parameter $M_\infty \sin\alpha$ is replaced by M_∞. In this paper, Barnwell's results are confirmed for sufficiently slender wings. In addition, a simple extension for not-so-slender wings and bodies is proposed and demonstrated for moderate angles of attack. A simple fit to the correlations based on the Polhamus suction analogy is demonstrated for several affine families of bodies with elliptical cross sections. The success of the extension suggests that useful simple models for nonlinear subsonic/transonic flows over not-so-slender wings and bodies can be built from a combination of well-known linear theory models for the attached flow and slender-body concepts for the vortical flow.

Nomenclature

A = coefficient for nonlinear normal force fit
AR = aspect ratio
a = semimajor axis of ellipse
B = exponent for nonlinear normal force fit
b = semiminor axis of ellipse
C = coefficient for nonlinear pitching moment fit; contour for calculation of circulation
C' = contour for calculation of circulation scaled by semispan
C_m = pitching moment coefficient normalized by planform area and body length
C_m^* = scaled pitching moment coefficient, $C_m/AR \sin\alpha \cos\alpha$
C_{m_v} = nonlinear portion of pitching moment coefficient
$C_{m_v}^*$ = scaled nonlinear portion of pitching moment coefficient, $C_{m_v}/AR \sin\alpha \cos\alpha$
C_{m_α} = slope of pitching moment coefficient at $\alpha = 0$
C_N = normal force coefficient normalized by planform area
C_N^* = scaled normal force coefficient, $C_N/AR \sin\alpha \cos\alpha$
C_{NL} = chordwise distribution of normal force coefficient
C_{NL}^* = scaled chordwise normal force coefficient distribution, $C_{NL}/AR \sin\alpha \cos\alpha$
C_{N_v} = nonlinear portion of normal force coefficient
$C_{N_v}^*$ = scaled nonlinear portion of normal force coefficient, $C_{N_v}/AR \sin\alpha \cos\alpha$
C_{N_α} = slope of normal force coefficient at $\alpha = 0$
c_p = pressure coefficient
D = exponent for nonlinear pitching moment fit
f = effective fineness ratio, $\ell/[2(a_{\max} b_{\max})^{\frac{1}{2}}]$
K_v = coefficient of nonlinear normal force coefficient term in suction analogy
k_1 = inner-flow similarity parameter, $\delta \cot\alpha$
k_2 = outer-flow similarity parameter for supersonic speeds, $M_\infty \sin\alpha$
k_3 = modified inner-flow similarity parameter, $\tan\alpha/AR$
ℓ = body length or wing chord
M_∞ = freestream Mach number; also outer-flow similarity parameter for subsonic/transonic speeds
p = static pressure
p' = scaled static pressure, $p/q_\infty \sin^2\alpha$
q_{cf} = crossflow velocity vector
q'_{cf} = scaled crossflow velocity vector, $q_{cf}/U_\infty \sin\alpha$
q_∞ = freestream dynamic pressure
s = local semispan
s_m = maximum semispan
S_p = planform area
u,v,w = flow velocity components in cylindrical coordinates
u',v',w' = scaled flow velocity components, $u/U_\infty \cos\alpha$, $v/U_\infty \sin\alpha$, $w/U_\infty \sin\alpha$, respectively
U_∞ = freestream velocity
x_{mc} = moment center for pitch
x,r,ϕ = cylindrical coordinates aligned with the body axis with origin at nose tip
x',r',ϕ' = scaled cylindrical coordinates, x/ℓ, r/s_m, ϕ, respectively
$\bar{x}$ = axial location of the center of pressure measured from apex
$\bar{x}_v$ = axial location of the center of pressure for the nonlinear portion of the normal force
y_v = spanwise location of vortex core measured from body axis
y_v^* = scaled spanwise location of vortex core, y_v/s_m

Presented as Paper 88-0216 at the AIAA Aerospace Sciences Meeting, Reno, NV, Jan. 11–14, 1988; received Feb. 19, 1988; revision received May 30, 1988.

*Engineering Specialist. Associate Fellow AIAA.

z_v = vertical location of vortex core
z_v^* = scaled vertical location of vortex core, z_v/s_m
α = angle of attack
β = Prandtl-Glauert similarity parameter, $|1-M_\infty^2|^{\frac{1}{2}}$
Γ = circulation
Γ^* = scaled circulation, $\Gamma/U_\infty s_m \sin\alpha$
Γ_C = circulation due to the core of a leading-edge vortex system
δ = slenderness parameter, s_m/ℓ
Δc_p = difference between lower and upper surface pressures
Δc_p^* = scaled surface pressure difference, $\Delta c_p/\delta \sin\alpha \cos\alpha$
ε = ellipticity of cross section
Λ = leading-edge sweep
ρ = density
ρ' = scaled density, ρ/ρ_∞
ρ_∞ = freestream density
σ_{v_r} = difference between the positions of the vortex and its image in the complex plane obtained by transforming the cross-sectional shape of the wing or body into a circle
$(\tan\alpha/AR)_0$ = value of k_3 at which significant vortex shedding begins

Introduction

HIGHLY blended slender airframes with arbitrary cross-sectional shapes are promising candidates for a variety of vehicles including high-performance tactical missiles, advanced fighter forebodies, supersonic and hypersonic transports, and single-stage-to-orbit launch vehicles. The simultaneous constraints of volume, drag, stealth, lift, and static and dynamic stability characteristics make it necessary for designers to use simple models to sort through the huge design space available. Unfortunately, the present lack of such models prevents full utilization of the design freedom afforded by arbitrary slender shapes.

This paper is the second in a series describing work that was undertaken to develop a basis for simple engineering design models suitable for slender wings and bodies at all speeds and for all angles of attack for which the flow is quasisteady. The first paper in the series[1] outlined the selected approach, which is based on the similarity analysis done by Sychev[2] in his development of hypersonic slender-body theory for arbitrary angles of attack. References 1 and 2 showed that time-like behavior in the axial direction holds for any steady flow over a sufficiently slender body at an arbitrary angle of attack, as long as the axial velocity component is supersonic and the flow features of interest are confined to a region near the body.

The accuracy and usefulness of Sychev's simplification of the governing equations were demonstrated in Ref. 1. In that paper, the similarity parameters deduced by Sychev were reviewed and used to correlate flowfield, surface pressure, normal force, and center-of-pressure data for supersonic flow over thin affine slender wings and smooth affine slender bodies at low-to-high angles of attack. A surprising result of the analysis was the discovery that one-term power law expressions could be used to accurately fit the normal force and center-of-pressure location correlations. This result suggested that it may be possible to develop a simple semiempirical method for estimating the aerodynamic characteristics of arbitrary slender airframes. In any case, the similarity analysis makes it possible to interpolate in and extrapolate from experimental and computational data bases in a natural and reliable way. Furthermore, it appears that the power law expressions in similarity variables give fits to experimental data that are superior to the two-term expressions normally used.

In the present paper, the methods of Ref. 1 are extended to moderate-angle-of-attack subsonic/transonic flows over thin slender wings and smooth slender bodies. In the first section, the Sychev similarity is reviewed and the appropriate changes for subsonic/transonic flow are described. The results are then applied to an affine family of gothic wings. In the second section, it is shown that the approach can be extended to not-so-slender wings and bodies, provided that slender-body similarity is applied only to the nonlinear, i.e., vortex-induced, portion of the loads. In the following sections, the extended similarity is applied to an affine family of elliptical cones and four affine families of power law bodies with elliptical cross sections. It is shown that the resulting correlations can be satisfactorily fit with a simple modification to the formula derived from the suction analogy.[3]

Extension of Sychev Similarity to Subsonic/Transonic Flows

In his analysis of the Euler equations for flow about an arbitrary slender body, Sychev assumed that

$$\delta \equiv s_m/\ell \ll 1 \tag{1}$$

and introduced the following dimensionless independent variables:

$$x' = x/\ell, \qquad r' = r/s_m, \qquad \phi' = \phi \tag{2}$$

and the dimensionless dependent variables

$$u' = u/U_\infty \cos\alpha, \qquad v' = v/U_\infty \sin\alpha$$
$$w' = w/U_\infty \sin\alpha, \qquad p' = p/q_\infty \sin^2\alpha, \qquad \rho' = \rho/\rho_\infty \tag{3}$$

All of the dimensionless variables are of order one. By substituting Eqs. (2) and (3), which effectively stretch the inner region, into the governing equations and boundary conditions and then dropping terms of second order and higher in δ, Sychev obtained an approximate set of equations and conditions for the inner region representing what he called a two-dimensional, unsteady flow analogy and involving only the parameter

$$k_1 = \delta \cot\alpha \tag{4}$$

Time is represented by the axial coordinate. Thus, a solution method that marches in the x direction can be used. For flows at high supersonic speeds, the flow disturbances lie close to the body and consideration of the bow shock wave is all that is needed to characterize the outer flow. Sychev's analysis shows that for slender bodies the reduced shock conditions depend only on k_1 and an additional similarity parameter, $k_2 = M_\infty \sin\alpha$.

For subsonic and transonic flows, the effect of the outer flow is not so easily treated, since the ellipticity of the flow must be retained. However, for most cases of interest, the lateral extent of the inner region is still $O(\delta)$ since the wake consists of vortical tubes which lie close to the body. Thus, k_1 is still the correct similarity parameter for the inner region. Furthermore, we can consider the outer flow to be governed by the full potential equation. Barnwell[4] has shown that the reduced form of the outer-flow potential equation does not depend on k_1 and the coefficients cannot be expressed simply as functions of $M_\infty \sin\alpha$. However, if it is assumed that

$$M_\infty \sin\alpha \ll 1 \tag{5}$$

then the outer-flow (Prandtl-Glauert) solution depends only on M_∞. The restriction on crossflow Mach number may seem extreme, but transonic crossflow will develop on most shapes of interest if Eq. (5) is violated. For such cases, a more

complex analysis similar to transonic lifting line theory[5] is likely to be appropriate.

The time-like nature of the reduced inner-flow equations has been exploited with considerable success in several engineering methods.[6–8] However, the investigators assumed rather than derived the governing equations. Also, the similarity parameter k_1 was used by Smith[9] in its small angle form in his slender-body theory studies of vortex sheet roll-up from the leading edges of low-aspect-ratio wings. It should be noted, however, that, since the inner region similarity arises out of a set of marching equations, we cannot expect a proper accounting of trailing-edge phenomena such as the Kutta condition and vortex breakdown. As in classical slender-body theory, airframes that give rise to such phenomena violate the assumed conditions of slenderness. However, it is shown below that effects due to the Kutta condition, at least, can be handled satisfactorily without losing the value of the similarity analysis.

For a perfect gas, the approximate relations derived by Barnwell[4] involve only the similarity parameters k_1 and M_∞ and the ratio of specific heats. As a consequence, for affine bodies in the same perfect gas, all of the dimensionless dependent variables are equal at corresponding points of the flowfield if k_1 and M_∞ have the same values for the two cases. For example, since we have

$$p' = p'(x',r',\phi',k_1,M_\infty) \tag{6}$$

it is easy to show for perfect gases that p/p_∞, $c_p/\sin^2\alpha$ and $c_p/\delta \sin\alpha \cos\alpha$ are also similarity variables and are functions of x', r', ϕ', k_1, and M_∞ only.

Integrating the pressure over the body surface gives

$$C_N/\sin^2\alpha = f_1(k_1,M_\infty) \tag{7}$$

$$C_M/\sin^2\alpha = g_1(k_1,M_\infty) \tag{8}$$

The above relations are somewhat inconvenient since the left-hand sides tend to infinity for small angles of attack. It is also more convenient for comparisons of different families of affine bodies to define the parameter

$$k_3 = \tan\alpha/\mathcal{A}\mathcal{R} = \text{const}/k_1 \tag{9}$$

Multiplying Eqs. (7) and (8) by k_3 and replacing k_1 with k_3, we have

$$C_N^* \equiv C_N/\mathcal{A}\mathcal{R} \sin\alpha \cos\alpha = f_2(k_3,M_\infty) \tag{10}$$

$$C_m^* \equiv C_m/\mathcal{A}\mathcal{R} \sin\alpha \cos\alpha = g_2(k_3,M_\infty) \tag{11}$$

Dividing Eq. (8) by Eq. (7) gives

$$\bar{x}/\ell = h_1(k_3,M_\infty) \tag{12}$$

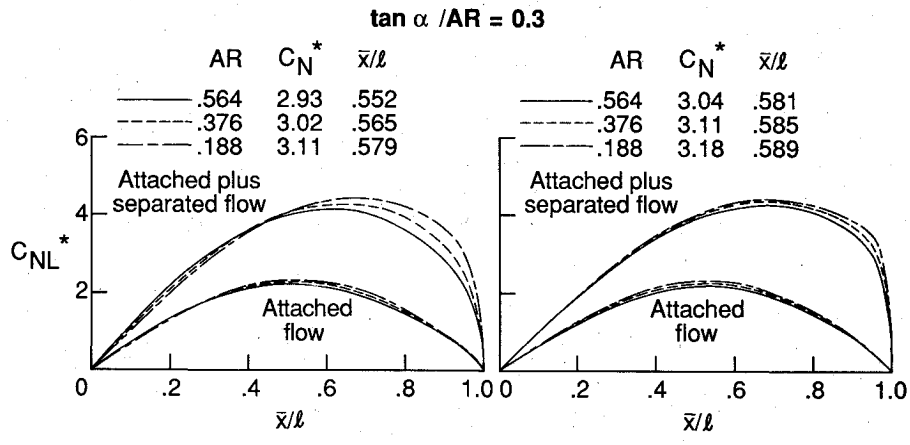

Fig. 1 Normal force load distributions for thin gothic wing family.

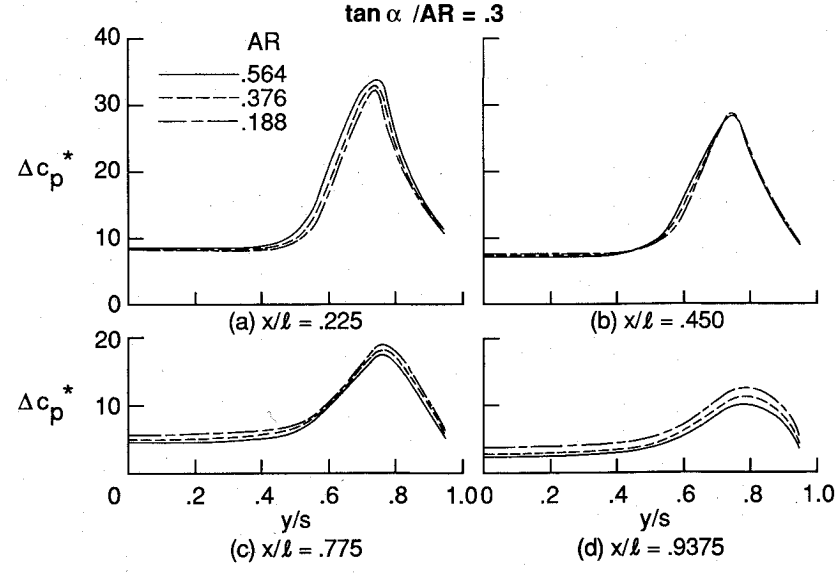

Fig. 2 Lifting-pressure coefficient for thin gothic wing family at $M_\infty = 0$.

which can be used in place of Eq. (11). It should be noted that the above similarity rules were derived from the Euler equations. Hence, in order for the rules to hold, the flows of interest must be, at most, weakly dependent on the Reynolds number.

Verification for Thin Slender Wings

For a wing to be mathematically "slender," all gradients in the flowfield in the axial (chordwise) direction must be smooth and small. This means that the semispan must change smoothly and gradually in the chordwise direction and end at the trailing edge in streamwise tips. Since the author was unable to find any systematic data for affine families of such wings, it was decided to perform a computational study using the free-vortex-sheet code.[10] The code solves the Prandtl-Glauert equation using higher-order quadrilateral panels to cover the wing surface and to represent rollup of the leading-edge vortex sheet. The thin wing planforms chosen for the study are gothic and are represented by

$$s/s_m = 0.5(3x - x^3) \tag{13}$$

A threefold aspect-ratio range of 0.188–0.564 was covered in the calculations. A k_3 value of 0.3 was used to obtain vortex-induced loads roughly equal to the attached flow loads. Chordwise loading results for incompressible flow and for $M_\infty = 0.95$ are given in Fig. 1. Note that the Sychev similarity scaling is accurate for both attached flows and for the $M_\infty = 0.95$ attached-plus-separated flow case. However, the scaling is significantly inaccurate for the incompressible attached-plus-separated flow case near the trailing edge. For this case (Fig. 1a), the variation of C_N^* over a threefold range of aspect ratio is only about 6%, but $\bar{x}/\ell$ varies about 2.7%. Spanwise lifting pressure loads for the incompressible case are given in Fig. 2. Note that the results are essentially similar with the larger discrepancies for $x/\ell = 0.9375$ corresponding to the larger discrepancies in chordwise normal force loading. Since the discrepancies are not uniform over the wing chord, but rather occur near the trailing edge, the center-of-pressure location will not scale well and will depend weakly but significantly on the aspect ratio.

In order to investigate similarity for the characteristics of the leading-edge vortex, several additional relations must be established. It is clear that the vortex positions in the crossflow plane are related by

$$y_v^* = y_v/s_m = y_v^*(x', k_3, M_\infty) \tag{14}$$

$$z_v^* = z_v/s_m = z_v^*(x', k_3, M_\infty) \tag{15}$$

Furthermore, the circulation for an arbitrary contour C in the crossflow plane is given by

$$\Gamma = \int_C \boldsymbol{q}_{cf} \cdot d\boldsymbol{t} \tag{16}$$

where $\boldsymbol{q}_{cf}$ is the crossflow velocity vector and $d\boldsymbol{t}$ is an infinitesimal arc length along C. Normalizing $\boldsymbol{q}_{cf}$ and $d\boldsymbol{t}$ according to Eqs. (2) and (3) gives

$$\Gamma^* = \int_{C'} \boldsymbol{q}'_{cf} \cdot d\boldsymbol{t}'$$

$$= \Gamma^*(x', K_3, M_\infty) \text{ on } C' \tag{17}$$

where $\Gamma^* = \Gamma/U_\infty s_m \sin\alpha$ and C' is the scaled contour for integration.

Vortex characteristics for incompressible flow for the gothic wings in this study are given in Fig. 3. Note that the scaling is very accurate, which raises the question of the source of the discrepancy shown in Figs. 1 and 2. It is shown in the next section that slender-body theory gives a Sychev similarity for the vortex-induced portion of the loads. Hence, it is likely that the assumptions of slender-body theory regarding vortices are inherent in the Sychev reduction of the Euler equations. Unfortunately, slender-body theory regards the vorticity vectors to be normal to the crossflow plane. This means that inclination of a vortex relative to the body axis is not accounted for in the velocity field. Thus, while the vortices scale in strength and position to first order, the fact that they are not aligned with the body axis creates a contribution to the axial velocity through the circumferential velocity field—a contribution that may not be properly scaled.

If the above conjecture is correct, the more slender members of an affine family of wings should have a higher scaled vortex loading because the greater sweep of the vortex contributes a smaller negative component to the axial velocity, as is shown in Fig. 1. Furthermore, a higher freestream Mach number should reduce the scaling discrepancy as is shown in Fig. 1b. The hypothesized scaling discrepancy due to vortex sweep would be strongest when the attached-flow loads are small compared to those induced by the vortex. Consequently, the effect will be strongest near the trailing edge and will cause the center of pressure due to vortex loading to move aft with decreasing aspect ratio and increasing Mach number, as shown in Fig. 1.

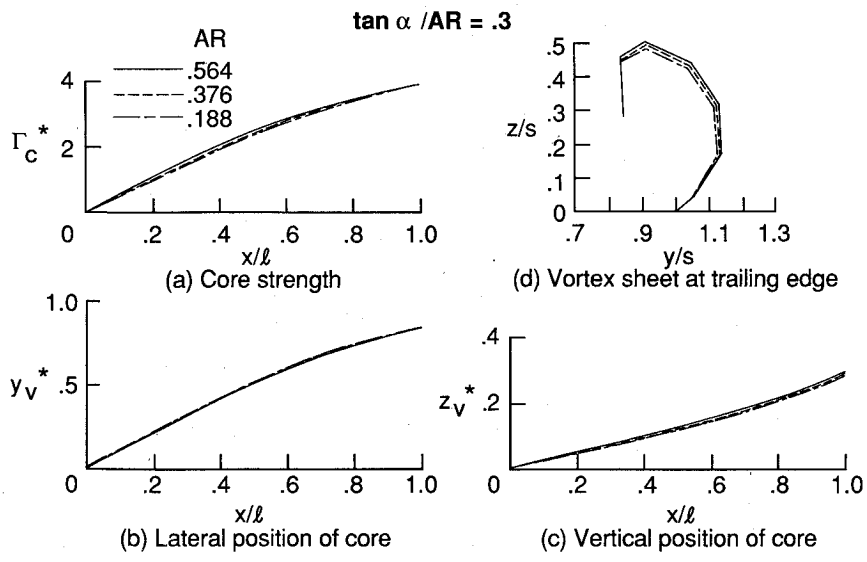

Fig. 3 Leading-edge vortex characteristics for thin gothic wing family at $M_\infty = 0$.

Extension to Wings and Bodies with Nonsimilar Attached Flows

The attached flow over most slender wings and bodies of interest does not satisfy similarity and it is necessary to account for this. Some insight into a satisfactory procedure for correcting for this lack of attached-flow similarity can be obtained by considering computational and experimental results for subsonic flow over delta wings. Several researchers have found that the velocity field of the primary vortex is nearly conical even though the wing surface pressure distribution is not.[11,12] This suggests that Sychev slender-body similarity may at least be applicable to the portion of the slender wing or body loading induced by the vortical flowfield. Computed results from the free vortex sheet code[10] for the vortex properties of several delta wings for $k_3 = 0.25$ and $M_\infty = 0$ are presented in Fig. 4. The range of leading-edge sweep angles corresponds to an aspect-ratio range of more than five. It can be seen that the accuracy of the similarity scaling for the vortex core properties is sufficient for engineering purposes.

The vortex properties and vortex-induced loading have been related by the slender-body analysis of Sacks.[13] According to Sacks, the increment in normal force coefficient acting on a slender wing or body due to shedding of a symmetric pair of vortices is given by

$$C_{N_v} = 2\cos\alpha\Gamma Re(\sigma_{v_r})/U_\infty S_p \tag{18}$$

where σ_{v_r} is the difference between the positions of the vortex and its image in the complex plane at the trailing edge obtained by transforming the cross-sectional shape of the body or wing into a circle. Substituting the vortex similarity equations (14), (15), and (17) into Eq. (18) gives

$$C^*_{N_v} \equiv C_{N_v}/AR\sin\alpha\cos\alpha = f_3(k_3, M_\infty) \tag{19}$$

which exhibits the same similarity dependency as Eq. (10). A companion result is easily obtained for the pitching moment coefficient. The development given above, of course, does not include Reynolds number effects, which are assumed to be weak. Also, because Sacks' analysis was made in the context of the slender-body theory approximation, the sweep effect of the leading-edge vortices on the velocity field is not taken into account.

A check on Eq. (19) has been made using the free vortex sheet code.[10] Solutions are given in Fig. 5 for thin delta wings

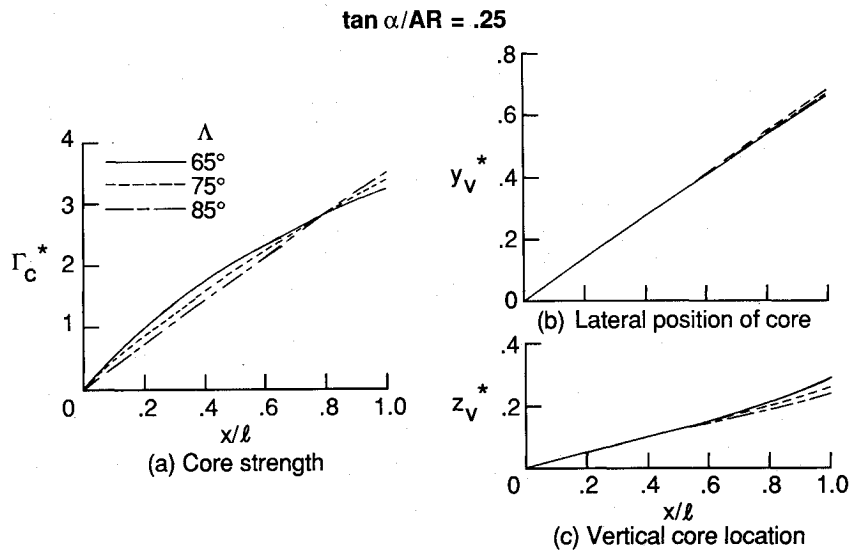

Fig. 4 Leading-edge vortex characteristics for thin delta wings at $M_\infty = 0$.

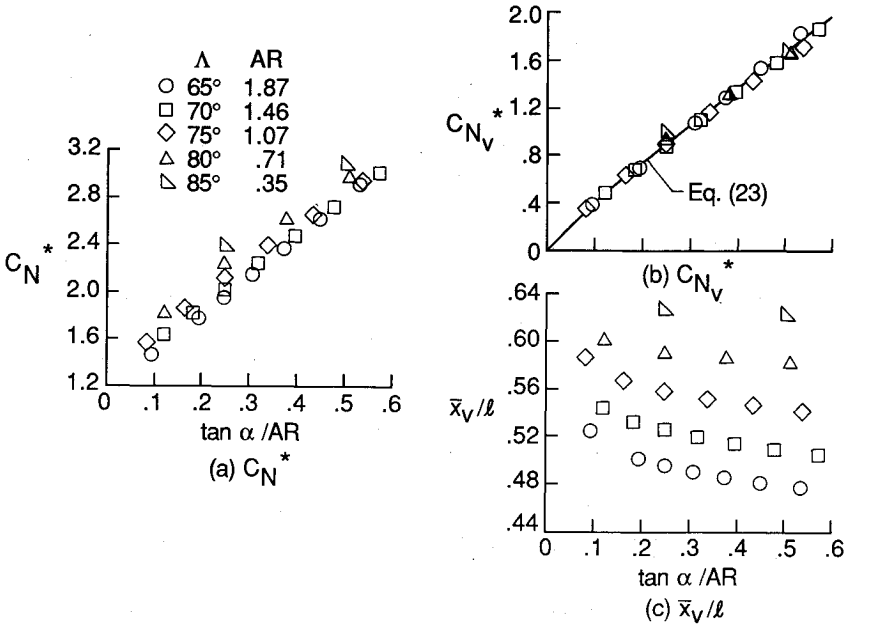

Fig. 5 Similarity for computational solutions for thin delta wings at $M_\infty = 0$.

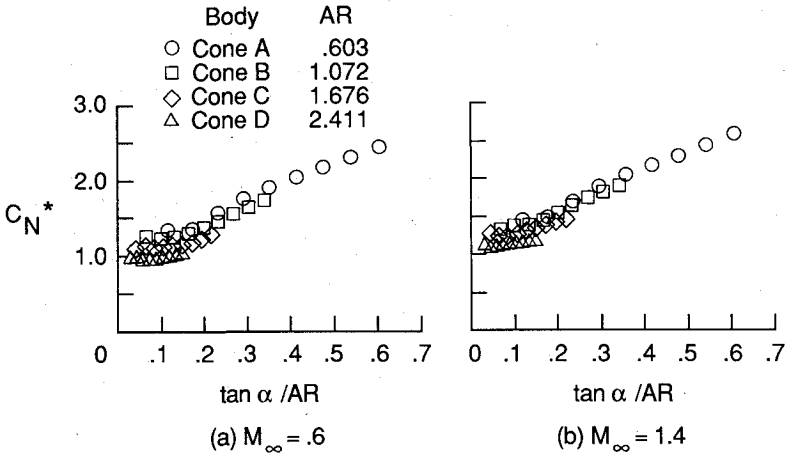

Fig. 6 Typical normal force similarity for elliptical cones ($\epsilon = 3$).

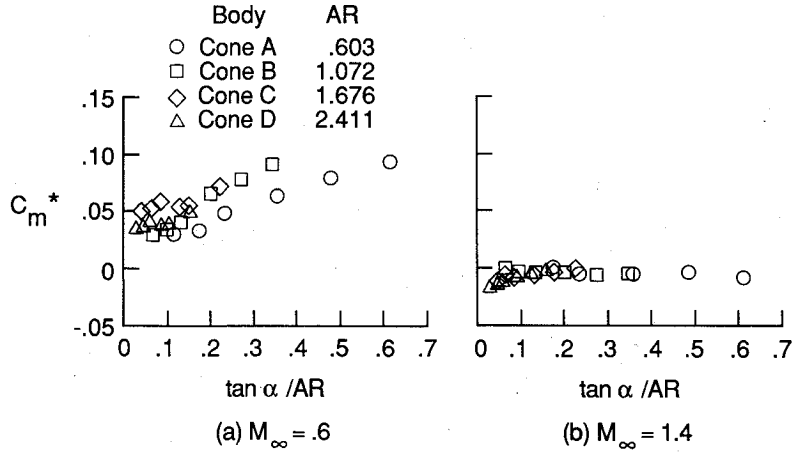

Fig. 7 Typical pitching moment similarity for elliptical cones ($\epsilon = 3$).

at $M_\infty = 0$ for angles of attack for which symmetric flow is expected. As usual, C_{N_v}, C_{m_v}, and $\bar{x}_v/\ell$ are defined by

$$C_N = C_{N_\alpha} \sin\alpha \cos\alpha + C_{N_v} \tag{20a}$$

$$C_m = C_{m_\alpha} \sin\alpha \cos\alpha + C_{m_v} \tag{20b}$$

$$\bar{x}_v/\ell = x_{mc} - C_{m_v}/C_N \tag{20c}$$

Figure 5 shows that similarity does not hold for C_N^*, but that scaling the nonlinear portion of the flow does produce the desired collapse of the data. It should be noted, however, that the center-of-pressure location for the nonlinear portion of the normal force coefficient does not scale very well. This is to be expected given the results presented in the previous section for slender gothic wings. This disappointing result means that the aspect-ratio range over which one can expect to scale or extrapolate subsonic pitching moment data is considerably smaller than it would be for supersonic flows.[1]

It is interesting to compare the Polhamus suction analogy[3] with the nonlinear normal force coefficient results of Fig. 5. According to the suction analogy, the normal force coefficient increment generated by the leading-edge vortices shed from a thin, sharp-edged wing is given by

$$C_{N_v} = K_v \sin^2\alpha \tag{21}$$

or, in similarity form,

$$C_{N_v}^* = K_v(\tan\alpha/AR) \tag{22}$$

which is a one-term power law expression with an exponent of one. For slender delta wings, the theoretical value of K_v ranges from π to approximately 3.2 for the aspect-ratio range considered in Fig. 5. The best one-term power law fit to the free vortex-sheet code results of Fig. 5 is given by

$$C_{N_v}^* = 3.07(\tan\alpha/AR)^{0.93} \tag{23}$$

which is nearly identical to the slender-wing suction analogy formula [Eq. (22)].

Application to Smooth Slender Bodies

Elliptical Cones

The extension of the previous section has been applied to an affine family of elliptical cones tested by Stivers and Levy[14] at subsonic and transonic speeds at angles of attack up to 20 deg. The cross-sectional ellipticity of the bodies was three and the aspect-ratio range was 0.6–2.4. The Mach number range was 0.6–1.4. Boundary-layer transition wires were placed around each model near the apex and along rays on the upper and lower surfaces near the leading edge. The Reynolds number was held constant at 1.4×10^6 based on model length and flow visualization was used to establish the effectiveness of the transition wires in producing a turbulent boundary layer.

Typical normal force and pitching moment similarity results for subsonic and supersonic cases are given in Figs. 6 and 7. The moment reference center is located at $\frac{2}{3}$ of the body length. It is obvious that similarity does not hold for attached flow over these cones. So, in order to use the extension of the previous section, the functions $C_{N_\alpha} \sin\alpha \cos\alpha$ and $C_{m_\alpha} \sin\alpha \cos\alpha$ were fitted to the small-angle-of-attack normal force and pitching moment data, respectively. The center-of-pressure location was then extracted from the data fits. The results are given in Figs. 8 and 9 as a function of the linear

Prandtl-Glauert similarity parameter βAR. Note that the supersonic C_{N_α} results do not satisfy linear theory similarity, probably because of transonic effects.

The nonlinear portions of the normal force and pitching moment coefficients were found by subtracting the linear portions obtained from the correlations of Figs. 8 and 9 from the data of Figs. 6 and 7. The correlated results are given in Figs. 10 and 11 for typical subsonic and supersonic Mach numbers. The correlations for $C^*_{N_v}$ are excellent. The simplest model with which to fit the correlations is just a slight modification of the suction analogy formula [Eq. (22)] to account for the delay in onset of vortex separation. The $C^*_{N_v}$ correlations for the Mach number range considered can be accurately fit by

$$C^*_{N_v} = A[\tan\alpha/AR - (\tan\alpha/AR)_0] \tag{24}$$

where $(\tan\alpha/AR)_0$ is an offset giving the angle of attack at which significant vortex shedding begins. The values of the offset for these elliptical cones are 0.15 and 0.12 for subsonic and supersonic flow, respectively. In general, A is not equal to K_v and $(\tan\alpha/AR)_0$ is greater than zero for smooth bodies and for wings with blunt leading edges.

The behavior of $C^*_{m_v}$ in Fig. 11 for the subsonic case is similar to that shown above for thin sharp-edged delta wings with the scaled center of pressure for nonlinear loading moving aft with decreasing aspect ratio. The simplest possible fit to the nonlinear pitching moment data is given by assuming a single value of $\bar{x}_v$ for each Mach number, thereby requiring the following form for $C^*_{m_v}$:

$$C^*_{m_v} = C[\tan\alpha/AR - (\tan\alpha/AR)_0] \tag{25}$$

where the normal force offsets are used. The value of C (and, hence, $\bar{x}_v$ was estimated by fitting a straight line to the higher angle-of-attack data points for the lowest-aspect-ratio body as shown in Fig. 11.

The values of A and $\bar{x}_v$ extracted from the correlations of Figs. 10 and 11 are given in Fig. 12 as a function of Mach number. Comparison of the original data with Eqs. (20), (24), and (25) using the fits of Figs. 8, 9, and 12 gives errors that are either less than the reported measurement accuracies or

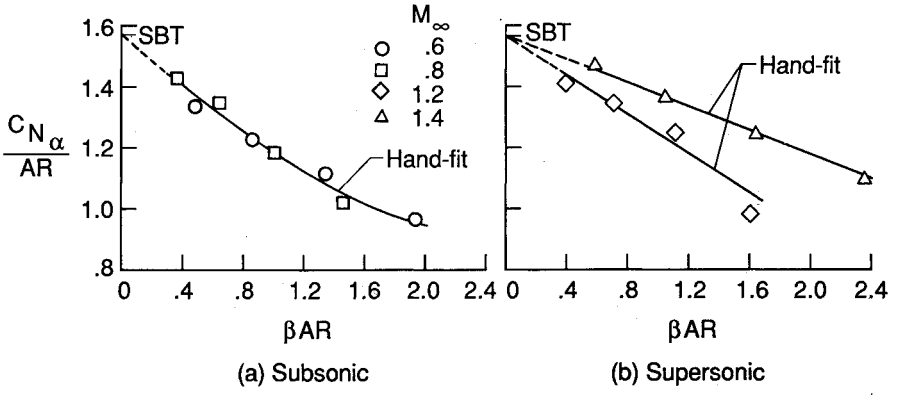

Fig. 8 Prandtl-Glauert similarity for slope of normal force coefficient for elliptical cones at $\alpha = 0(\epsilon = 3)$.

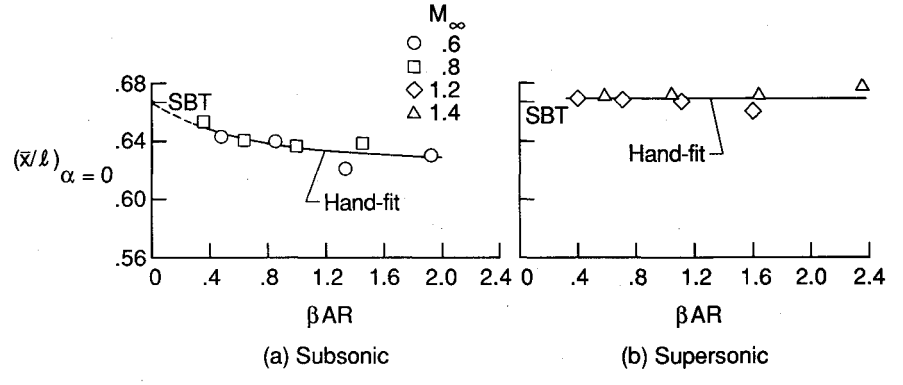

Fig. 9 Prandtl-Glauert similarity for center-of-pressure location for elliptical cones at $\alpha = 0(\epsilon = 3)$.

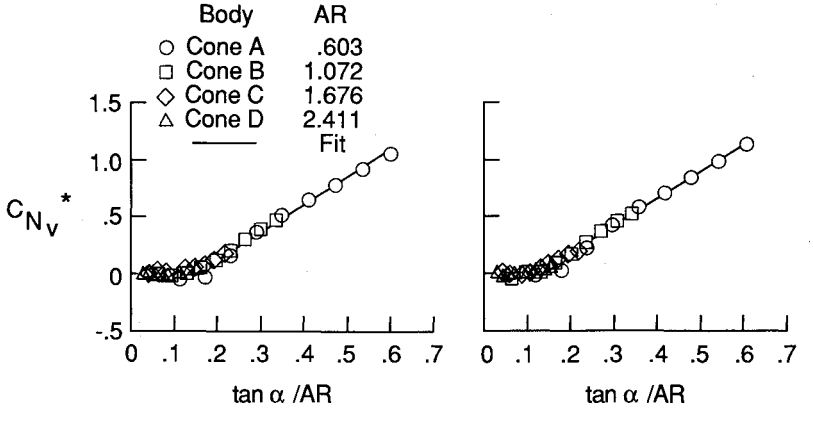

Fig. 10 Similarity for nonlinear portion of normal force coefficient for elliptical cones ($\epsilon = 3$).

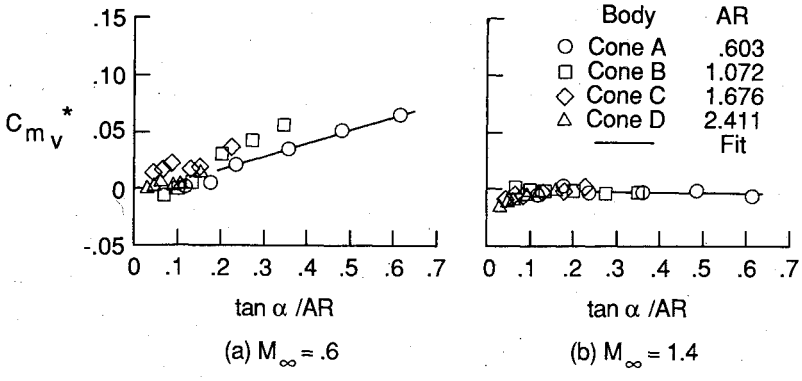

Fig. 11 Similarity for nonlinear portion of pitching moment coefficient for elliptical cones ($\epsilon = 3$).

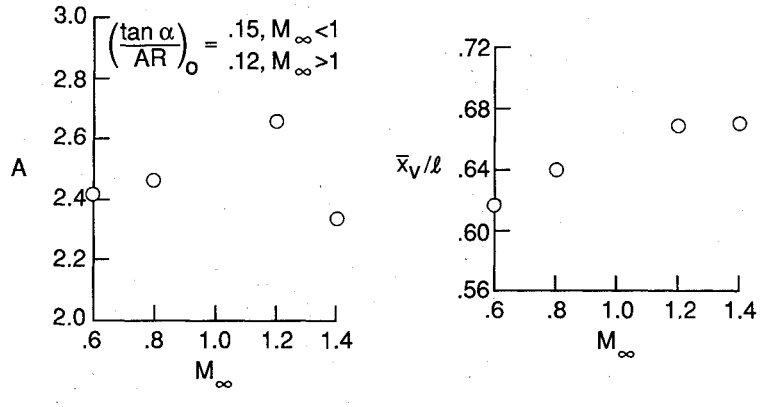

Fig. 12 Mach number dependence of similarity fits for elliptical cones ($\epsilon = 3$).

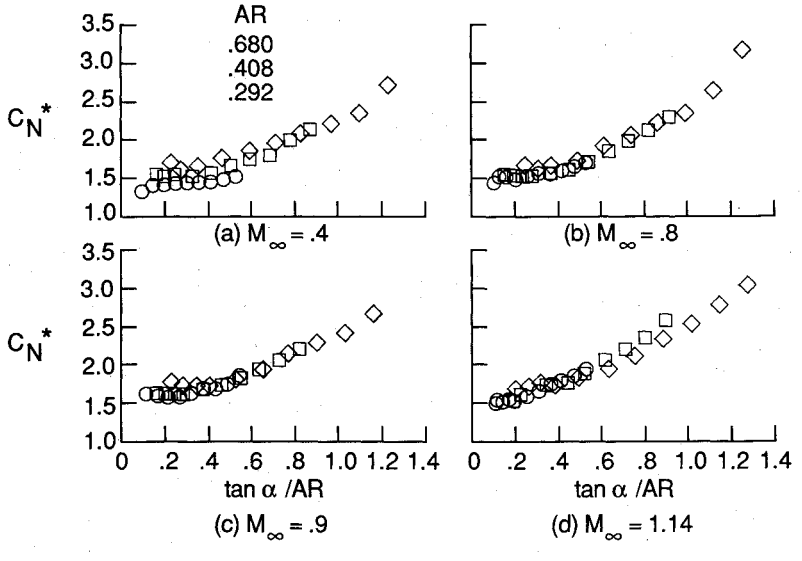

Fig. 13 Normal force similarity for power law bodies with $\epsilon = 1.5$ for Mach number range.

are less than about 5% for normal force. For pitching moment, the maximum errors above the measurement accuracies represent errors of about 2 and 1% of the body length for subsonic and supersonic flows, respectively.

Power Law Bodies

The approach of the previous section has also been applied to four affine families of power law bodies with elliptical cross sections. The body planforms are represented by

$$s/s_m = (x/\ell)^{\frac{2}{3}} \tag{26}$$

The bodies were tested by Spencer and Phillips[15] at subsonic and transonic speeds for angles of attack up to 20 deg. The Mach number range was 0.4–1.14. The four affine families had ellipticity ratios of 0.5, 1.0, 1.5, and 2.0. Within each family there were three bodies with effective fineness ratios of 3, 5, and 7. The effective fineness ratio f was computed using the diameter of an axisymmetric base with the same cross-sectional area. All bodies had the same base area and a single balance was used to measure all forces and moments. Transition was fixed by grit bands near the apex and along the body length on the lower surface near the leading edge. Since measurement errors were not estimated, it has been assumed that the measured coefficients are accurate to within 1% of the maximum values reported.

Typical normal force and pitching moment similarity results are given in Figs. 13–16. The moment reference center is located at $\frac{2}{3}$ of the body length. It is evident from the correlations that the power law bodies act as if they are more

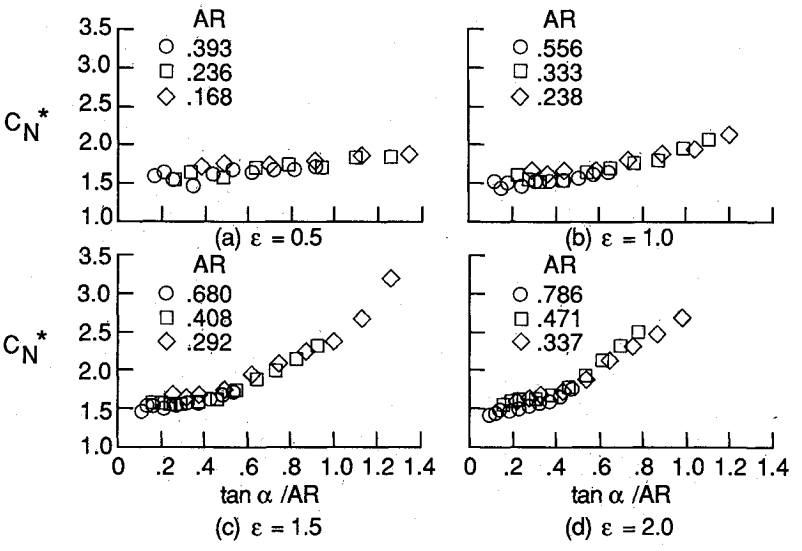

Fig. 14 Normal force similarity for power law bodies at $M_\infty = 0.8$ for ellipticity range.

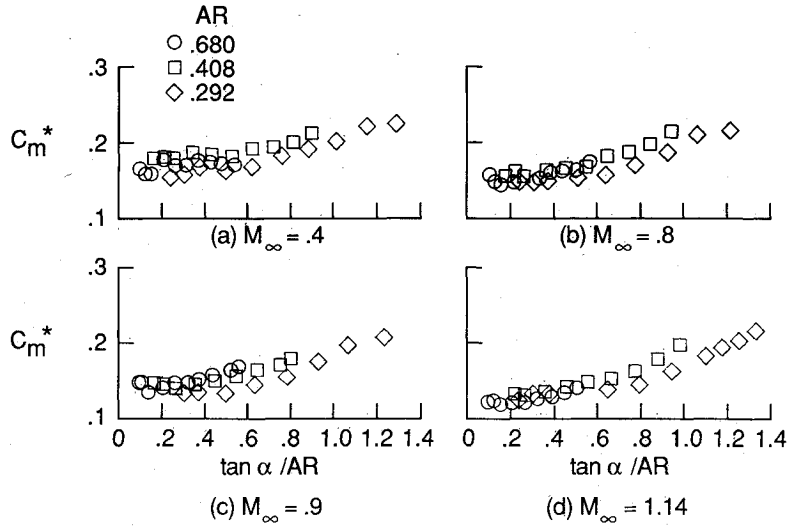

Fig. 15 Pitching moment similarity for power law bodies with $\epsilon = 1.5$ for Mach number range.

"slender" than the elliptical cones of the previous section. The subsonic correlations exhibit characteristics similar to those of the cones and Eqs. (24) and (25) can be used for fitting, but the supersonic cases appear to require fits of the more general form

$$C^*_{N_v} = A(\tan\alpha/\mathcal{AR})^B \tag{27}$$

$$C^*_{m_v} = C(\tan\alpha/\mathcal{AR})^D \tag{28}$$

where A, B, C, and D are all functions of M_∞.

The correlated subsonic data of Figs. 13–16 were fit using the procedure of the previous section. The Prandtl-Glauert similarity results are given in Fig. 17 and the nonlinear similarity results are given in Fig. 18. Since all of the planforms are affine and classical slender-body theory predicts that the normal force generated by a body with elliptical cross sections depends only on the span and not the ellipticity of the cross section, single fits were used for the Prandtl-Glauert correlations for all four ellipticity families. Most of the scatter for the center-of-pressure correlation in Fig. 17 is due to balance inaccuracies since the bodies with lower values of ε have smaller planform areas and, hence, generate smaller values of normal force.

Within the accuracy of the data, the similarity correlation fit parameters $(\tan\alpha/\mathcal{AR})_0$, A, and $\bar{x}_v/\ell$ are independent of freestream Mach number ($M_\infty < 1$). In addition, the data inaccuracies made it impossible to directly estimate $(\tan\alpha/\mathcal{AR})_0$ for the family with $\varepsilon = 0.5$. Instead, since the formula

$$(\tan\alpha/\mathcal{AR})_0 = 0.55\varepsilon^{-0.65} \tag{29}$$

represents the correlations for $\varepsilon > 0.5$ fairly well, it was used to estimate the offset for $\varepsilon = 0.5$.

The variation of the parameter A with ellipticity is also easily represented and is given by

$$A = \varepsilon - 0.2 \tag{30}$$

The scatter for the parameter $\bar{x}_v/\ell$ is too large for determining a satisfactory formula. The solid line shown in Fig. 18c was obtained by fairing through the values averaged over Mach number. The line was simply extrapolated for ellipticity valued below one.

Comparison of the original data for all four families (12 bodies) with the fits of Figs. 17 and 18 gives errors that are either less than the estimated measurement accuracies or less than about 9% for normal force. For pitching moment, the maximum errors were on the order of the estimated measurement accuracies or less than about 2.5% of the body length.

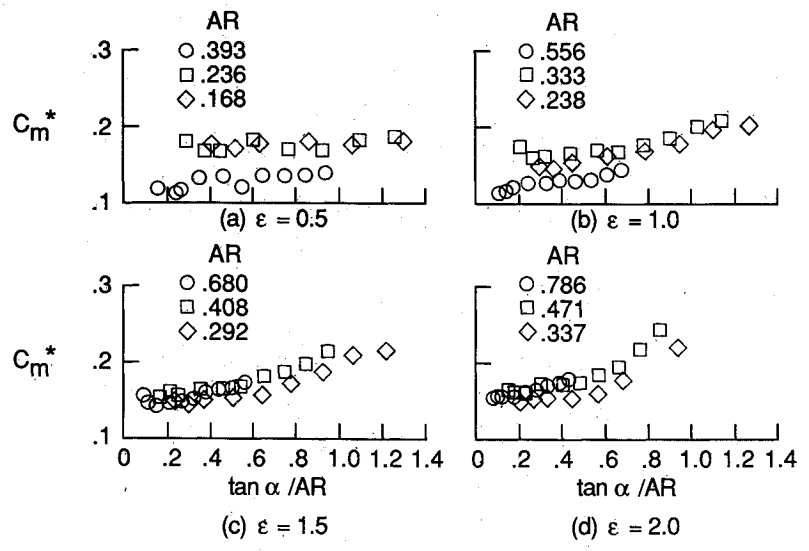

Fig. 16 Pitching moment similarity for power law bodies at $M_\infty = 0.8$ for ellipticity range.

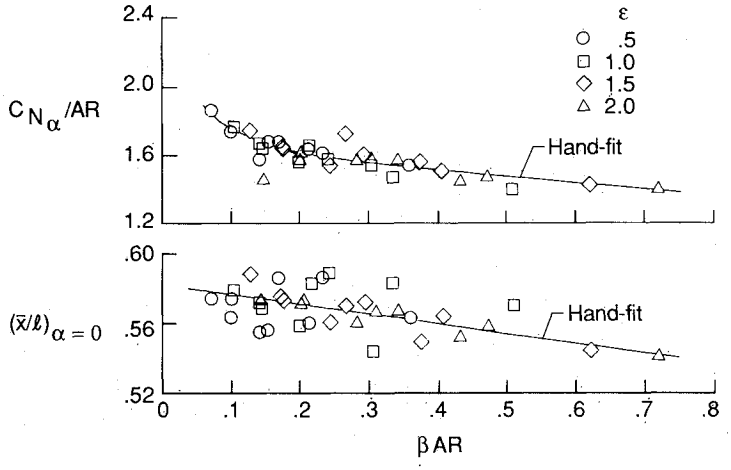

Fig. 17 Prandtl-Glauert similarity for slope of normal force coefficient and for center-of-pressure location for power law bodies at subsonic speeds ($\alpha = 0$).

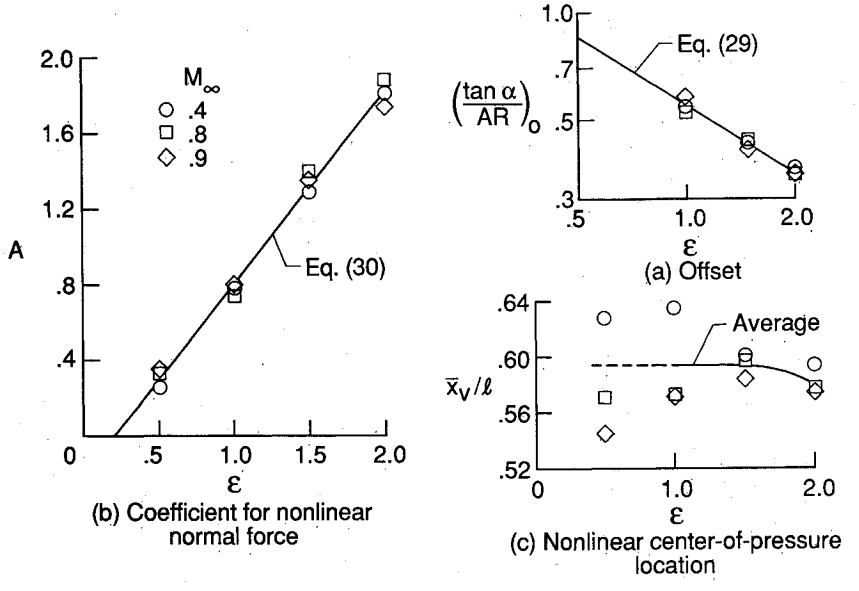

Fig. 18 Dependence of similarity fits on ellipticity for power law bodies for subsonic speeds.

Concluding Remarks

The similarity analysis developed by Sychev[2] for inviscid hypersonic flow over slender bodies and extended to subsonic and transonic flows by Barnwell[4] has been applied to sharp-edged wings and smooth bodies. By applying the analysis to thin gothic slender wings it was found that, while the normal-force scaling works well, the scaled vortex-induced loading shifted aft significantly with decreasing aspect ratio for subsonic Mach numbers. This effect causes the pitching moment correlations to be weakly, but significantly, dependent on aspect ratio. This means that the wide aspect-ratio correlation range achieved for supersonic flows[1] is necessarily smaller for subsonic flows for the pitching moment.

For not-so-slender wings and bodies, i.e. airframes for which the attached flow does not have Sychev similarity, it was found that the vortex-induced portion of the loads can be satisfactorily scaled. Furthermore, a simple modification of the Polhamus suction analogy[3] formulas to include delay in the onset of vortex shedding can be used to fit the resulting correlations for subsonic flows. The extension for not-so-slender bodies was successfully applied to an affine family of elliptical cones and four affine families of power law bodies with elliptical cross sections.

An important conclusion implicit in the results presented is that subsonic vortical flows of the sort studied here can be simply modeled as a combination of Prandtl-Glauert similarity for the attached flow and extended Sychev similarity for the vortical flow. This suggests that, for design purposes, a high-angle-of-attack flow with a well-defined vortex system can be successfully modeled by superimposing a combination of an elliptic attached flow and a parabolic vortical flow. However, the approach has been confirmed only for separated flows composed of symmetric vortex pairs. In addition, it is unlikely that flows with vortex breakdown can be modeled this way—except, perhaps, for the flow upstream of the breakdown position.

Acknowledgments

Support of the Advanced Configurations Branch of NASA Langley Research Center under Contract NAS1-18000 is gratefully acknowledged. Helpful discussions with Drs. R. W. Barnwell and J. M. Luckring and Mr. E. C. Polhamus are also gratefully acknowledged. Dr. Luckring provided the free vortex sheet code solutions from which Figs. 4 and 5 were obtained.

References

[1]Hemsch, M. J., "Engineering Analysis of Slender-Body Aerodynamics Using Sychev Similarity Parameters," *Journal of Aircraft*, Vol. 25, July 1988, pp. 625–631.

[2]Sychev, V. V., "Three-Dimensional Hypersonic Gas Flow Past Slender Bodies at High Angles of Attack," *Journal of Applied Mathematics and Mechanics* (*USSR*), Vol. 24, Feb. 1960, pp. 296–306.

[3]Polhamus, E. C., "A Concept of the Vortex Lift of Sharp-Edged Delta Wings Based on a Leading-Edge Suction Analogy," NASA TN D-3767, 1966.

[4]Barnwell, R. W., "Extension of Hypersonic, High-Incidence, Slender-Body Similarity," *AIAA Journal*, Vol. 25, Nov. 1987, pp. 1519–1522.

[5]Cheng, H. K. and Meng, S. Y., "Lifting-Line Theory of Oblique Wings in Transonic Flow," *AIAA Journal*, Vol. 17, Jan. 1979, pp. 122–124.

[6]Mendenhall, M. R. and Perkins, S. C., Jr., "Vortex Cloud Model for Body Vortex Shedding and Tracking," *Tactical Missile Aerodynamics, AIAA Progress in Astronautics and Aeronautics*, Vol. 104, edited by M. J. Hemsch and J. N. Nielson, AIAA, Washington, DC, 1986, Chap. XII.

[7]Nathman, J. K., "Analysis of Leading-Edge Vortices on Complex Configurations," AIAA Paper 85-4054, Oct. 1985.

[8]Sacks, A. H., Lundberg, R. E., and Hanson, C. W., "A Theoretical Investigation of the Aerodynamics of Slender Wing-Body Combinations Exhibiting Leading-Edge Separation," NASA CR-719, March 1967.

[9]Smith, J. H. B., "Improved Calculations of Leading-Edge Separation from Slender Delta Wings," Royal Aeronautical Establishment, TR-66070, March 1966.

[10]Tinoco, E. N., Lu, P., and Johnson, F. T., "An Improved Panel Method for the Solution of Three-Dimensional Leading-Edge Vortex Flows," NASA CR-3279, July 1980.

[11]Thomas, J. L. Taylor, S. L., and Anderson, W. K., "Navier-Stokes Computations of Vortical Flows Over Low Aspect Ratio Wings," AIAA Paper 87-0207, Jan. 1987.

[12]Carcaillet, R., Manie, F., Pagan, D., and Solignac, J. L., "Leading Edge Vortex Flow Over a 75 Degree Swept Delta Wing—Experimental and Computation Results," International Congress of Aeronautical Sciences, Vol. I, Sept. 1986, pp. 589–603.

[13]Sacks, A. H., "Vortex Interference on Slender Airplanes," NACA TN 3525, Nov. 1955.

[14]Stivers, L. S., Jr. and Levy, L. L., Jr., "Longitudinal Force and Moment Data at Mach Numbers from 0.60 to 1.40 for a Family of Elliptical Cones with Various Semiapex Angles," NASA TN D-1149, 1961.

[15]Spencer, B., Jr. and Phillips, W. P., "Transonic Aerodynamic Characteristics of a Series of Bodies Having Variations in Fineness Ratio and Cross-Sectional Ellipticity," NASA TN D-2622, Feb. 1965.